Investigating the Influence of Plant Fiber Geometry on Apparent Transverse Elastic Properties through Finite Element Analysis

Jason Govilas[a], Cédric Clévy[a], Johnny Beaugrand[b], Vincent Placet[a]

[a] Université de Franche-Comté, CNRS, institut FEMTO-ST, 25000, Besançon, France

[b] INRAE, UR 1268 BIA Biopolymères Interactions Assemblages, 44316 Nantes, France

Abstract

This study explores the link between plant fiber geometry and its transverse behavior, focusing on the resulting apparent transverse stiffness as determined by analytical models. Using Finite Element Analysis (FEA) plant fiber transverse compression is simulated with two-dimensional models. Simplified geometric representations of common geometric features are examined, showing how distinct attributes influence behavior. The fiber lumen is shown to decrease apparent stiffness, while elliptical geometry and flat sections increase it. An adaptation of analytical models for elliptical cross-sections yields a 93% improvement on identification accuracy. Furthermore, the transverse compression of realistic geometries, extracted from microscopy images and presenting a blend of different features, is simulated. The lumen's impact on apparent stiffness is shown to outweigh the effects of other features. These findings show the importance of apparent stiffness over fiber cell wall stiffness and how it may evolve under repeated loading, which has important implications for the composites sector.

Keywords: A. Natural fibers, B. Elasticity, C. Finite element analysis (FEA), D. Mechanical testing

1. Introduction

In the continuous effort towards sustainable materials the adoption of plant fibers as an alternative to their synthetic counterparts (glass, carbon, aramid, polymer) presents significant environmental benefits, due to their renewability, biodegrability, light weight and more [1][2]. Structural applications are of particular interest, a notable example being the use of plant fibers as composite reinforcements [3][4]. Among the various available plant fibers, bast fibers such as flax, hemp and nettle are of particular interest for such applications, since their structural role within the fiber leads to high mechanical properties [5].

Nevertheless, accurate knowledge of plant fiber mechanical properties is necessary in order to favor their wider adoption in structural applications [6].

Direct mechanical testing at the fiber scale, while challenging due to the small size of fibers, can reliably characterize plant fiber mechanical properties compared to indirect testing methods [7]. Among such tests, tensile testing has been performed extensively, providing the longitudinal properties of various plant fibers [8–11]. However, to the authors knowledge the transverse properties of plant fibers have never been determined through direct testing. This constitutes a major bottleneck in the development and modeling of plant fiber reinforced composites. The established way to characterize transverse properties at the fiber scale is the Single Fiber Transverse Compression Test (SFTCT). This test has been performed on various synthetic fibers such polymer [12–18] aramid [19–24] or carbon fibers [25,26] and to the authors knowledge, only once on natural materials, with the compression of wood fibers [27].

The principle of a SFTCT is simple: a single fiber is rested on a stationary platen while a mobile one compresses it. Despite this apparent simplicity however, the gradual increase in contact surface between fibers and platens leads to a non-linear material behavior of the fiber, even if it is considered purely elastic and isotropic, preventing a direct estimation of material parameters. For this reason, analytical models have been developed for SFTCTs, relating fiber morphology and material characteristics to the applied compressive force and fiber contraction during compression [12,15,19,21]. Such models allow for the identification of fiber transverse material parameters, notably the transverse elastic modulus E_T, through identification by inverse method.

While these models present some minor differences, they all consider the fiber as a right circular cylinder. The considerably larger length of fibers compared to their diameters, allows for a plane strain hypothesis to be made, making the models 2D, with only a circular fiber section being modeled. The manufacturing processes used for synthetic fiber production leads to fiber geometries that are overall homogenous and consistent and can thus be assimilated to right circular cylinders. The geometry of plant fibers on the other hand is significantly more complex [6]. Plant fibers present an intrinsic central porosity, called the lumen [28]. Lumen size can vary significantly between plant species. The limited space inside the plant's stem, where plant fibers grow, lead to further intricate geometric features. Circular cross sections lead to a sub-optimal use of the space inside the stem, plant fiber cross sections thus grow into intricate cross sections instead, making use of the available space. Furthermore, as fibers get in contact during

growth, their cross sections can become flatter over the areas in contact. Overall, plant fiber cross sections are closer to elliptical, or even polygonal as opposed to circular, as can be seen in the cross section of part of a hemp stem in Figure 1.a. In addition to their cross section complexity, plant fibers also exhibit geometric variations and twist along their length [28,29] further differentiating them from perfect cylinders.

Given the morphological complexity of plant fibers, the validity of using existing SFTCT analytical models, to predict plant fiber behavior and identify their transverse properties by inverse method, remains an open question. In the case of tensile testing, the influence of fiber morphology on measured properties has been studied by comparing cross section area measurement methods [29,30]. Finite Element Analysis (FEA) represents an alternative to analytical models since it can account for significantly more complexity, being geometric or material, at the expanse of the simplicity and ease of use of analytical models. Numerous simulations of complex plant fiber geometries have been performed in the case of tensile testing [31–40], however to the authors knowledge no such study exists in the case of transverse compression. Simulating SFTCTs of plant fibers would provide valuable inside on the influence the various geometric parameters on fiber behavior. Comparing FEA results with analytical model predictions would also provide answers on the validity of the latter in the case of plant fiber transverse compression.

In this paper, the SFTCT of 2D geometries representing the transverse section of plant fibers is simulated with FEA. In this way the 2D assumptions of the analytical models are kept and only cross section geometric complexity is added, allowing for a comprehensive study of its influence on fiber behavior. An adaptation of existing analytical models to account for elliptical cross sections is also proposed and validated, offering a geometrically richer analytical model. Employing the data generated by the FEA, an apparent transverse elastic modulus, E_T^{app}, is identified using the new analytical model. The influence of fiber geometry on this apparent modulus evaluated and discussed. Ideal geometric representations of the fiber's most common geometric features are studied first, to independently assess their effect on fiber behavior and apparent modulus. Specifically, the influences of lumen size, ellipticity and flat fiber sections are evaluated. Furthermore, the transverse compression of complex plant fiber geometries, extracted from microscopy images with a custom algorithm, is simulated. The impact of the interplay between various geometric features on fiber behavior and apparent modulus is thus evaluated on a more experimentally representative case.

2. Materials and methods

2.1. Common plant fiber geometric feature ideal representations

Three main geometric characteristics of plant fibers are studied in idealized, symmetric geometric representations: the lumen, fiber ellipticity and fiber flat sections. Due to this symmetric assumption, one a quarter of the fiber is considered. The lumen is represented as concentric circle of radius R_L in a circular fiber of radius R, as seen in Figure 2.a. Ellipticity is studied through perfect elliptical fiber geometries, with a minor radius R and major radius R_m as pictured in Figure 2.b. The major radius is parallel to the compression platens, while the minor radius is in the direction of compression. An ellipse flattening factor f can be calculated with:

$$f = 1 - R/R_m \quad (1)$$

Flat sections are represented by combining a rectangle of width w and an elliptical fiber with a minor radius $R - w$ and a major radius R, as seen in Figure 2.c.

The influence of these geometric characteristics on the identification of E_T is studied by varying the ratios R_L/R, and w/R or the ellipse flattening f from 0, in the case of a perfectly circular fiber, to 0.9 with R remaining constant. As a result, the same fiber radius is compressed in all studies.

2.2. Microscopy extracted fiber geometries

In order to study realistic plant fiber cross sections, that are inherently much more complex than their ideal geometry counterparts, fiber geometries are extracted from a microscopy image, using a similar method to those presented in [36,41,42]. An observation of a hemp stem section is used for this purpose, shown in Figure 1.a. After binarization of the image using Otsu's thresholding method [43] the contours of the image are detected using the *bwboundaries* function of MATLAB (MathWorks, Natick, MA) as seen in Figure 1.b.

With the contours in the image being detected, the contour of a cell wall can be isolated. The largest contour contained within the cell wall (the lumen's boundary) can also be isolated if visible. The contour detection algorithm results in fine irregularities in the extracted geometries (see Figure 1.c and d) that can be problematic in FEA. For this reason, after converting to polar coordinates, a smoothing spline is applied

to the cell wall and lumen contours, eliminating fine detail while maintaining the overall fiber morphological complexity[1]. The smoothing on polar coordinates along with the final smoothed geometry can be seen in Figure 1.c and Figure 1.d respectively. Overall, a morphologically diverse set of 20 fibers with varying sizes and shapes, with or without lumens, are chosen for FEA, shown in Figure 3.

2.3. Analytical model adaptation and inverse identification

For the inverse identification of E_T, the analytical model developed by Jawad et al. [15] is used, which considers the fiber as a cylinder of radius R in plane strain conditions. To adapt to elliptical geometries, a simple modification of the model is proposed, employing the major radius R_m and the minor radius R. Considering that the ellipse is compressed along its major or minor axis, the radius that is parallel to the platens will greatly influence the width of the contact zone between the fiber and the platens. On the other hand, the fiber's contraction will be influenced by the radius that is perpendicular to the platens, in the direction of compression, this radius will thus be used in the rest of the model.

During the initial phase of compression, plant fibers often slide and rotate during a partial compression phase, under the influence of the upper compression platen's movement. This partial compression phase usually leads to a configuration where their major radius is parallel to the platens as seen in Figure 4. In such a configuration, the fiber is less likely to rotate and full compression takes place. Under this configuration, the analytical model can be written as followed with the major radius R_m being used in the calculation of contact half-width b and the minor radius R in the rest of the model.

$$U = \frac{4F_L}{\pi}\left[\left(\frac{1}{E_T} - \frac{\nu_{LT}^2}{E_L}\right)\left(sinh^{-1}\left(\frac{R}{b}\right) + ln(2)\right) - \frac{1}{2}\left(\frac{1}{E_T}(1-\nu_{TT}^2) - 2\frac{\nu_{LT}^2}{E_L}\right)\right.$$
$$\left. + \left(-\frac{\nu_{TT}^2}{E_T} - \frac{\nu_{LT}^2}{E_L}\right)\frac{R}{b}\left(\sqrt{1+\left(\frac{R}{b}\right)^2} - \frac{R}{b}\right)\right] \quad (2)$$

[1] Centering the data with respect to 0° greatly helps the smoothing procedure. Once the smoothing is performed, coordinates can be moved back to their initial position.

$$b = \sqrt{\frac{4FR_m}{\pi}\left(\frac{1}{E_T} - \frac{\nu_{LT}^2}{E_L}\right)} \quad (3)$$

with: U: the displacement of the fiber, F_L: the force per unit length, E_L: the fiber's longitudinal elastic modulus, E_T: the fiber's transverse elastic modulus and ν_{LT}, ν_{TT}: the Poisson ratios in the longitudinal and transverse plane respectively.

For the microscopy-extracted geometries, after fitting an ellipse over the cell wall contour, the same configuration is desired. A rotation is applied to the ellipse and the fiber, to position the major ellipse axis horizontally as seen in Figure 5.a. The major radius of the fitted ellipse is used for the calculation of b with the minor radius being used in the rest of the analytical model. The fiber can be rotated further by the user, if the resulting configuration could still lead to important fiber rotation during compression, to a configuration where full compression is more likely (see Figure 5.b). While minimizing fiber rotations during compression, this additional rotation can lead to identification errors if the major axis of the fiber and the fitted ellipse become very misaligned.

The presented analytical model is used to identify an apparent transverse elastic modulus E_T^{app} from FEA data through a least-squares regression analysis as detailed in [44]. The relative difference between the apparent fiber transverse elastic modulus, E_T^{app}, identified by the analytical model, and transverse elastic modulus defined in the FEM, E_T, is calculated:

$$\Delta E_T = \frac{E_T^{app} - E_T}{E_T} \quad (4)$$

Positive values of ΔE_T indicate an increased apparent fiber stiffness compared to the fiber's actual stiffness, since $E_T^{app} > E_T$. Inversely, negative values of ΔE_T indicate a decreased apparent stiffness. To calculate how closely the analytical model reproduces fiber behavior, the average value of the least-squares residual is calculated:

$$\rho = \frac{1}{N}\sqrt{\sum_{i=1}^{N}(U_i^{FEA} - U_i^{AN})^2} \quad (5)$$

where: N: the number of FEA data points, U^{FEA}: the upper platen displacement in the FEA and U^{AN}: the fiber displacement predicted by the analytical model.

Finally, to evaluate the accuracy of the proposed elliptical model its values of ΔE_T and ρ are compared to those obtained with the conventional model when the major or minor radius is used as an input. Results from the transverse compression of elliptical fibers are used, with an ellipse flattening factor f varying from 0 to 0.9.

2.4. Finite element model

In order to evaluate the influence of plant fiber geometry on the identification of E_T, FEMs of the previously described fiber geometries under transverse compression, are created in COMSOL Multiphysics © (COMSOL AB, Stockholm, Sweden). With the exception of geometry, the rest of the modeling choices made by the analytical model are respected: a 2D plane strain formulation is used, compression platens are rigid and parallel, while the fiber is modeled as elastic and transversely isotropic. To match the infinitesimal strain approach of the analytical models, a linear strain formulation is use. Therefore, any difference between the values of E_T that are imposed in the FEM or identified by the analytical model can be attributed to the differences in geometry.

For the study of ideal geometric representations, fiber geometry is considered symmetric along both the xz and yz plane, therefore only a quarter of the fiber is modeled (see Figure 6.a). A radius value of $R = 16\ \mu m$ is chosen, which representative of average plant fiber diameters [45]. In the case of microscopy-extracted geometries, the entire cross section is modeled. By determining the pixel size, the size of the microscopy-extracted fibers corresponds to the one found in the microscopy image.

For all the fibers studied, the fiber's longitudinal modulus is set at $E_L = 50\ GPa$, which is in the order of magnitude of common bast fibers such as flax, hemp and nettle [6,46]. The transverse elastic modulus is set at $E_T = 1\ GPa$ according to preliminary experimental SFTCTs [47]. Poisson ratios have been shown to have very little influence on fiber behavior under SFTCT and subsequent E_T identification [23,44]. Values are thus set arbitrarily at $\nu_{LT} = 0.4$ and $\nu_{TT} = 0.07$.

To simulate the transverse compression of a fiber, a maximum displacement of $1\mu m$ is imposed on the upper compression platen. A Lagrangian contact formulation between the platens and the fiber is used, with the platens as the masters, being the stiffer material. The force per unit of length F_L resulting from the fiber's compression is obtained by integrating the contact pressure's vertical component over the contact zone. For microscopy-extracted geometries where no symmetry conditions apply, the movement of the

lowest point on the fiber is blocked to eliminate potential rigid body movements (see Figure 6.b). A lower, fixed compression platen is also modeled in this case. Microscopy-extracted geometries can also be subject to some rotation at the start of the compression. These points are eliminated and the zero-displacement value of the platen is considered for the first point where no rotation occurs.

For the mesh of the fiber, triangular elements are chosen, allowing an easy adaptation of the mesh to any complex morphology. A quadratic shape function is used. A constant element size is used across all studies to avoid time consuming, given the number of different tested geometries, manual refinement steps. For ideal geometries, an element length of $R/26$ is chosen after a mesh refinement study, where ΔE_T converges at a value of $2.8 \cdot 10^{-4}\%$ for a fiber with a circular cross section. For microscopy extracted geometries an element size of $\bar{R}/26$ where $\bar{R}$ is the average of the fitted ellipse's major and minor radius. Given, their rectangular nature compression platens are meshed using structured quadrilaterals. Since the platens are the masters in the contact pairs with the fiber, elements that are two times bigger than the fiber are used. An overview of the boundary conditions and mesh for an ideal and microscopy-extracted geometry is given in Figure 6.

3. Results and discussions

3.1. Elliptical analytical model

Figure 7 illustrates ΔE_T and ρ values, for fibers with an ellipse flattening factor f, varying from 0 to 0.9. For all elliptical geometries, the identified transverse elastic modulus is overestimated regardless of the analytical model used in the identification, as attested by the positive values of ΔE_T (see Figure 7.a). The nature of this overestimation will be discussed in the next subsection. It can become very significant as fibers get more elliptical. For example, a flattening ratio of $f = 0.85$ leads to ΔE_T that surpass 100% for all analytical models. Nevertheless, the elliptical model leads consistently to lower values of ΔE_T. The use of the original model leads to higher values of ΔE_T, especially when the major radius is used as an input instead of the minor radius.

Across all studied ellipse flattening factors the elliptical model leads to an average decrease in ΔE_T of $93 \pm 24\%$ (mean value and standard deviation) compared to the conventional model with the minor radius as an input, and $185 \pm 47\%$ (mean value and standard deviation) when the major radius is used as an input.

The relative difference in ΔE_T between the original and elliptical model stays relatively stable up until $f = 0.8$, where differences in ΔE_T become more important, which explains the rather large standard deviation values. Similar trends can be observed for the average least-squares identification residual ρ, with the use of the major radius leading to highest values, followed by the use of the minor radius and the lowest values being obtained with the elliptical model, as seen in Figure 7.b. Residual values stay under 5 nm when the elliptical model is used, or 0.5% of the imposed displacement. The elliptical model thus reproduces fiber behavior accurately.

Overall, the use of the proposed elliptical analytical model leads to a significant improvement in both the identification of the fiber's transverse elastic modulus and the fitting of the model to the FEA data. It is thus the model of choice for all the following studies. If the original analytical model must be used, the value of the radius along the axis that is perpendicular to the platens, in our case the minor radius, should be preferred.

3.2. Ideal geometric representations

The vertical stress fields σ_{yy} resulting from the simulation of the ideal representations of the main plant fiber geometric characteristic are shown in Figure 8. A perfectly circular fiber with no lumen (see Figure 8.a) is depicted along with fibers with a lumen, an elliptical geometry or flat section with ratios R_L/R, f and w/R of 0.35 (see Figure 8.b) and 0.7 (see Figure 8.c). For a circular and full fiber, stresses are concentrated in the contact zone with the platens. The same is true for elliptical and flattened fibers however as contact zones are larger, stresses are spread over a wider zone and stress levels are generally lower. An exception can be seen for flat fibers, where high concentration levels occur at the interface between the flat and elliptical section. The presence of the lumen leads to two separate zones of stress concentrations: one close to the contact zone at the base of the lumen. This new stress concentration zone is explained by the compaction of the lumen that takes place during the fiber compression. Furthermore, an important decrease in maximum stress levels can be observed, that gets more important as lumen size grows. This increase in fiber compliance is also a result of the lumen compaction, which adds a structural displacement to the fiber displacement related to material deformation.

The force-displacement results obtained from the FEA analysis are shown in Figure 9. The decrease in stress levels for a given displacement, resulting from the presence of the lumen, leads to an important

decrease in force level (see Figure 9.a). On the other hand, both elliptical and flat-section geometries lead to an increase in force for a given displacement level, compared to a circular fiber, due to the increased contact zones related to these geometries (see Figure 9.b and Figure 9.c).

These changes in force levels, compared to the circular and full fiber case, have an influence on the identification of E_T by the analytical model, as seen by the values of ΔE_T in Figure 10.a. For elliptical and flat fibers, the increase in force leads to an overestimation of the transverse elastic modulus of the fiber ($\Delta E_T > 0$). For flat fibers ΔE_T increases almost linearly, by approximately 30% per increment of 0.1 of the ratio w/R. For elliptical geometries ΔE_T increases exponentially with low values for less elliptical fibers ($\Delta E_T < 10\%$ for $f < 0.3$ and $\Delta E_T < 40\%$ for $f < 0.6$). For more elliptical fibers ΔE_T rises rapidly, approaching values of 200%. However, for all tested geometries, ΔE_T resulting from elliptical geometries remain lower than flat-section geometries. For fibers with lumens, due to the decrease in force, ΔE_T values are negative, the identified apparent transverse modulus is thus lower than the modulus defined in the FEM. The evolution of ΔE_T follows a sigmoid-like trend with low values for smaller lumens, ($|\Delta E_T| < 10\%$ for $R_L/R < 0.2$) and higher values for large lumens ($|\Delta E_T| > 80\%$ for $R_L/R > 0.6$) that stabilize towards values of 100%. For intermediate lumen values ($0.2 < R_L/R < 0.6$) ΔE_T decreases more rapidly.

An important distinction in the interpretation of ΔE_T, for fibers with or without a lumen, must be noted. When no lumen is present, fiber displacement is a direct result of material deformation. Differences between the fiber's apparent modulus and the one imposed in the simulation occur because the model is developed for circular cross sections. Flat sections are not considered, while ellipticity is accounted for with a simple approximation. Therefore, in this case ΔE_T can be interpreted as the identification error made by the analytical model. For fibers with lumens however, structural displacement related to the lumen's compaction is added to material deformation. In this case, ΔE_T represents the difference between the transverse elastic modulus of the fiber's cell wall and the apparent modulus, identified by the analytical model. This apparent modulus is equivalent to the modulus of a full fiber with the same compliance as the fiber with a lumen. Within a structural application, fiber behavior will be dictated by both the material and structural displacement. Therefore, when a lumen is present, the apparent modulus might be of more interest than the modulus of the fiber wall itself and ΔE_T should not be interpreted as an identification error.

Fiber geometry also influences fiber behavior non-linearity, as seen in Figure 9. The non-linearity remains unchanged for elliptical geometries in general but also for smaller lumen sizes and flat sections. In

these cases, the analytical model reproduces this fiber behavior well. For larger lumen sizes and flat sections, the fiber response becomes more linear, which the analytical model does not reproduce as well. The analytical model's ability to fit the FEA data is given by the least-squares identification average residual, ρ, in Figure 10.b. For elliptical and flat-section fibers, residual values remain under $10nm$, which corresponds to 1% of the upper platen's maximum displacement, attesting to a good quality fit. For fibers with a lumen, residual values rise with an accelerated rate, as a function of lumen size. For $R_L/R = 0.9$, residual values reach $54nm$, or 5.4% of the maximum displacement. Therefore, the analytical model's ability to reproduce fiber behavior when a lumen is present, is worse than for elliptical or flat-section geometries. The added structural displacement related to lumen compaction is the reason, since it is not accounted for at all in the model's formulation.

Based on these identification results, an antagonist behavior becomes apparent between plant fiber geometric characteristics. Lumens lead to a decrease in apparent stiffness compared to the fiber cell wall stiffness. On the other hand, elliptical and flat geometries lead to an increase in apparent stiffness. Plant fibers are characterized by complex geometries that often present all of these characteristics. The value of E_T that is identified by the analytical model will depend on the overall interaction between these parameters.

3.3. Microscopy-extracted geometries

The force-displacement results of the FEA on microscopy-extracted fiber geometries is given in Figure 11. Depending on the fiber geometry, force levels can be quite diverse. Nevertheless, a clear trend can be observed, depending on the presence of a lumen in the fiber. Fibers with lumens consistently lead to lower force levels compared to those with no lumen. These differences in force level lead to a clear trend in the identified transverse elastic modulus as attested by the values of ΔE_T shown in Figure 12.a. A clear distinction can be made on the values of ΔE_T based on the presence of the lumen. All fibers with a lumen lead to decreased apparent stiffness ($\Delta E_T < 0$) while fibers with no lumen lead to an increased one ($\Delta E_T > 0$) with the exception of fiber 10. Given that studied fibers often have both elliptical and flat features but also a lumen (see Figure 3), it can be assumed that the lumen's decreasing effect on apparent fiber stiffness outweighs the increasing effect of elliptical and flat geometries.

Average and standard deviation values of ΔE_T are of $19.4 \pm 19.9\%$ for fiber with no lumen and $-28.9 \pm 24.6\%$ for fibers with a lumen. When all fibers are considered, the average value of ΔE_T is of

$-7 \pm 33\%$. Therefore, if a morphologically diverse set of fibers in tested with SFTCTs within a small deformation and elastic regime, the proposed elliptical analytical model can lead to small differences between apparent stiffness and fiber cell wall stiffness. The value of the standard deviation, while high compared to the average value, remains of the same order of magnitude as those found experimentally on identified plant fiber properties such as the tensile modulus and strength [8,46,48,49]. This points to plant fiber morphological diversity being one of the most predominant factors in the variability of their measured properties.

Regarding the ability of the analytical model to reproduce the behavior of complex fiber geometries, it can be seen in Figure 11 that the model fits well to the FEA data, for all tested fibers. This attested by the values of the least-squares identification residual, ρ, shown in Figure 12.b. All values remain under $6nm$, while the average value is of $2.5nm$, or 0.25% of the maximum imposed displacement. The standard deviation value is also low at $1.3nm$. Therefore, for plant fiber transverse compression performed within a small strain and elastic regime, existing analytical SFTCT with the added elliptical approximation are be able to reproduce fiber behavior even for complex geometries.

Considering, the effect the fiber's lumen, ellipticity and flat sections have on its apparent stiffness, a discussion can be made on the consequences of different loading modes on the fiber. If the fiber is loaded up to complete lumen compaction, a gradual increase in the identified apparent transverse elastic modulus could be observed as the lumen shrinks and structural displacement related compliance decreases. Once the lumen is completely compacted and the fiber's cell wall are in contact, an important increase should be observed. This compression would also increase the elliptical nature of the fiber, but also create an increasingly large flat zone, where contact with the platens occurs, contributing further to an increase in apparent stiffness. If a repeated loading is applied that results in irreversible deformations a change in apparent stiffness could also be expected. If the lumen compacts irreversibly during one cycle, less structural displacement will take place on the next, making the fiber appear stiffer. Irreversible deformations would also mean that the fiber would get more elliptical and flatter with each loading cycle. The combination of these mechanisms should result in an increase of the identified apparent transverse elastic modulus as a function of loading cycle, as long as damage mechanisms are not activated.

The discussed mechanisms could lead to important differences between the apparent transverse properties of single fibers, tested before any treatment; and fibers that have been subject to important or

repeated transverse loads during transformation and manufacturing processes. Plant fiber extraction such as scutching [6] or composite compression molding [50] are examples of such processes. If the lumen collapses irreversibly fiber with an increased apparent stiffness will be obtained. However, if the lumen does not collapse and is preserved in the final applications, structural displacements linked to its compaction will affect the fiber behavior and lead to lower apparent stiffness. In that case, the apparent transverse elastic modulus, which is identified by a model considering the fiber as full and thus encompasses both material and structural compliance, might be of more interest compared to the properties of the fiber cell wall itself.

4. Conclusions

In this paper, the influence of plant fiber geometry on its transverse behavior under SFTCT is investigated using FEA. The results of the FEA are used to identify by inverse method an apparent fiber transverse elastic modulus, using analytical models making simple geometric approximations. This apparent modulus is compared to the one imposed in the FEM through the relative difference ΔE_T. The ability of the analytical model to reproduce fiber behavior is also evaluated through the average least-squares regression residual.

An adaptation of existing analytical models was proposed to account for elliptical fiber cross sections. Based on simulation results from elliptical fibers under transverse compression, the newly proposed analytical model showed an average improvement of 93% on the accuracy of the identified transverse elastic modulus E_T, compared to the conventional analytical model that considers a circular fiber cross section.

Ideal representations of fibers with three common geometric characteristics were studied, to independently asses their impact on fiber behavior and apparent properties. Elliptical geometries and flat sections, lead to an increase in contact zone width which results in an increase in force for a given displacement. An increase in apparent stiffness occurs ($\Delta E_T > 0$), that can reach up to 268% and 185% for ratios of 0.9 for w/R and f respectively. For fibers with a lumen the compaction of the lumen leads to a structural displacement in addition to the fiber's cell wall deformation. The fiber is thus more compliant and force levels decrease for a given displacement. Consequently, a decrease in apparent stiffness occurs ($\Delta E_T < 0$), that can reach up to -100% for R_L/R =0.9.

Complex fiber geometries, extracted from microscopy images with a custom algorithm, were also studied enabling the study of the interaction between geometric parameters in a realistic manner. The decrease in force related to lumen compaction is shown to surpass the increase in force related to elliptical and flat features. The transverse elastic modulus identified by the analytical model is thus higher by 19.4% on average than the fiber's cell wall when no lumen exists and lower by 28.9% when a lumen is present. In general, the analytical model was shown to identify E_T values that are close to those of the fiber cell walls with an average ΔE_T value of -7%. Furthermore, its ability to reproduce the behavior of geometrically complex fiber was demonstrated by its close fit to the FEA data.

These results also suggest that existing analytical models with the proposed elliptical cross section approximation, can be used with satisfactory accuracy for the identification of plant fiber transverse properties through SFTCTs, when performed in an elastic and small strain regime. Nevertheless, analytical developments to improve their accuracy and considering more geometric features could be considered. Studying the influence of geometric variations along the fiber's length, with three-dimensional FEM, or inelastic fiber behavior would further verify their validity and provide additional insides on plant fiber transverse behavior. The proposed finite element models, could also represent an alternative to analytical models for the identification of fiber material properties. With the use of the microscopy-extracted geometries, complex and rich finite element models could be developed that would offer unprecedented accuracy in terms of behavior prediction and fiber cell wall property identification.

Finally, these results emphasize the importance of morphological and structural effects in plant fiber transverse behavior and apparent stiffness. Under repeated loading, if irreversible deformations take place, an increase in fiber apparent stiffness can occur as they get more elliptical and flatter or due to the lumen's collapse. Furthermore, if plant fibers are integrated into other materials, their apparent stiffness is of particular importance, encompassing both lumen compaction and fiber cell wall deformation. Lumen collapse within the material could significantly alter its behavior, by increasing the apparent stiffness of the embedded fibers. Inducing lumen collapse in fibers before their integration, could be explored to achieve stiffer or more stable materials. By considering these findings, researchers and engineers can make informed decisions when incorporating plant fibers into various materials, enhancing our ability to design materials with tailored properties to meet diverse needs.

Acknowledgements

These works have been supported by the European Union's Horizon 2020 research and innovation program under grant agreement No 771134. The project NETFIB was carried out under the ERA-NET Cofund SusCrop (Grant N°771134), being part of the Joint Programming Initiative on Agriculture, Food Security and Climate Change (FACCE-JPI). This work has also been supported by EIPHI Graduate School under ("ANR-17-EURE-0002").

[1] Joshi S V., Drzal LT, Mohanty AK, Arora S. Are natural fiber composites environmentally superior to glass fiber reinforced composites? Compos Part A Appl Sci Manuf 2004;35:371–6. https://doi.org/10.1016/j.compositesa.2003.09.016.

[2] Mansor MR, Mastura MT, Sapuan SM, Zainudin AZ. 11 - The environmental impact of natural fiber composites through life cycle assessment analysis. Durab. Life Predict. Biocomposites, Fibre-Reinforced Compos. Hybrid Compos., Woodhead Publishing; 2019, p. 257–85. https://doi.org/10.1016/B978-0-08-102290-0.00011-8.

[3] Mohanty AK, Vivekanandhan S, Pin JM, Misra M. Composites from renewable and sustainable resources: Challenges and innovations. Science (80-) 2018;362:536–42. https://doi.org/10.1126/science.aat9072.

[4] Gholampour A, Ozbakkaloglu T. A review of natural fiber composites: properties, modification and processing techniques, characterization, applications. vol. 55. Springer US; 2020. https://doi.org/10.1007/s10853-019-03990-y.

[5] Bourmaud A, Beaugrand J, Shah DU, Placet V, Baley C. Towards the design of high-performance plant fibre composites. Prog Mater Sci 2018;97:347–408. https://doi.org/10.1016/j.pmatsci.2018.05.005.

[6] Bourmaud A, Beaugrand J, Shah DU, Placet V, Baley C. Towards the design of high-performance plant fibre composites. Prog Mater Sci 2018;97:347–408. https://doi.org/10.1016/j.pmatsci.2018.05.005.

[7] Shah DU, Nag RK, Clifford MJ. Why do we observe significant differences between measured and 'back-calculated' properties of natural fibres? Cellulose 2016;23:1481–90. https://doi.org/10.1007/s10570-016-0926-x.

[8] Baley C, Bourmaud A. Average tensile properties of French elementary flax fibers. Mater Lett 2014;122:159–61. https://doi.org/10.1016/j.matlet.2014.02.030.

[9] Placet V, Cissé O, Lamine Boubakar M. Nonlinear tensile behaviour of elementary hemp fibres. Part I: Investigation of the possible origins using repeated progressive loading with in situ microscopic observations. Compos Part A Appl Sci Manuf 2014;56:319–27. https://doi.org/10.1016/j.compositesa.2012.11.019.

[10] Wang G, Shi SQ, Wang J, Yu Y, Cao S, Cheng H. Tensile properties of four types of individual cellulosic fibers. Wood Fiber Sci 2011;43:353–64.

[11] Yu Y, Jiang Z, Fei B, Wang G, Wang H. An improved microtensile technique for mechanical characterization of short plant fibers: A case study on bamboo fibers. J Mater Sci 2011;46:739–46. https://doi.org/10.1007/s10853-010-4806-8.

[12] Hadley D., Ward I., Ward J. The transverse compression of anisotropic fibre monofilaments. Proc R Soc London Ser A Math Phys Sci 1965;285:275–86. https://doi.org/10.1098/rspa.1965.0103.

[13] Pinnock PR, Ward IM, Wolfe JM. The compression of anisotropic fibre monofilaments. II. Proc R Soc London Ser A Math Phys Sci 1966;291:267–78. https://doi.org/10.1098/rspa.1966.0094.

[14] Morris S. 39—The Determination of the Lateral-Compression Modulus of Fibres. J Text Inst 1968;59:536–47. https://doi.org/10.1080/00405006808660016.

[15] Jawad SA, Ward IM. The transverse compression of oriented nylon and polyethylene extrudates. J Mater Sci 1978;13:1381–7. https://doi.org/10.1007/BF00553190.

[16] Kotani T, Sweeney J, Ward IM. The measurement of transverse mechanical properties of polymer fibres. J Mater Sci 1994;29:5551–8. https://doi.org/10.1007/BF00349946.

[17] Jones MCG, Lara-Curzio E, Kopper A, Martin DC. The lateral deformation of cross-linkable PPXTA fibres. J Mater Sci 1997;32:2855–71. https://doi.org/10.1023/A:1018672400459.

[18] Stamoulis G, Wagner-Kocher C, Renner M. Experimental study of the transverse mechanical properties of polyamide 6.6 monofilaments. J Mater Sci 2007;42:4441–50. https://doi.org/10.1007/s10853-006-0655-x.

[19] Phoenix S, Skelton J. Transverse Compressive Moduli and Yield Behavior of Some Orthotropic, High-Modulus Filaments. Text Res J 1974:934–40. https://doi.org/doi:10.1177/004051757404401203.

[20] Singletary J, Davis H, Song Y, Ramasubramanian MK, Knoff W. Transverse compression of PPTA fibers. Part I. Fiber transverse structure. J Mater Sci 2000;35:583–92. https://doi.org/10.1023/A:1004716108638.

[21] Cheng M, Chen W, Weerasooriya T. Experimental investigation of the transverse mechanical properties of a single Kevlar® KM2 fiber. Int J Solids Struct 2004;41:6215–32. https://doi.org/10.1016/j.ijsolstr.2004.05.016.

[22] Lim J, Zheng JQ, Masters K, Chen WW. Mechanical behavior of A265 single fibers. J Mater Sci 2010;45:652–61. https://doi.org/10.1007/s10853-009-3979-5.

[23] Wollbrett-Blitz J, Joannès S, Bruant R, Le Clerc C, De La Osa MR, Bunsell A, et al. Multiaxial mechanical behavior of aramid fibers and identification of skin/core structure from single fiber transverse compression testing. J Polym Sci Part B Polym Phys 2016;54:374–84. https://doi.org/10.1002/polb.23763.

[24] Sockalingam S, Bremble R, Gillespie JW, Keefe M. Transverse compression behavior of Kevlar KM2 single fiber. Compos Part A Appl Sci Manuf 2016;81:271–81. https://doi.org/10.1016/j.compositesa.2015.11.032.

[25] Kawabata S. Measurement of the transverse mechanical properties of high-performance fibres. J Text Inst 1990;81:432–47. https://doi.org/10.1080/00405009008658721.

[26] Naito K, Tanaka Y, Yang JM. Transverse compressive properties of polyacrylonitrile (PAN)-based and pitch-based single carbon fibers. Carbon N Y 2017;118:168–83. https://doi.org/10.1016/j.carbon.2017.03.031.

[27] Mikczinski M, Nguyen HX. Assessing Transverse Fibre Properties : Fibre Compression and Artificial Hornification By Periodic Compression. Adv Pulp Pap Res Trans XVth Fundam Res Symp Cambridge 2013:803–20. https://doi.org/10.15376/frc.2013.2.803.

[28] Richely E, Durand S, Melelli A, Kao A, Magueresse A, Dhakal H, et al. Novel insight into the intricate shape of flax fibre lumen. Fibers 2021;9. https://doi.org/10.3390/fib9040024.

[29] Garat W, Corn S, Le Moigne N, Beaugrand J, Bergeret A. Analysis of the morphometric variations in natural fibres by automated laser scanning: Towards an efficient and reliable assessment of the cross-sectional area. Compos Part A Appl Sci Manuf 2018;108:114–23. https://doi.org/10.1016/j.compositesa.2018.02.018.

[30] Thomason JL, Rudeiros-Fernández JL. Modelling the influence of fibre internal structure on the measured modulus of technical natural fibres. Compos Part A Appl Sci Manuf 2021;147:106478. https://doi.org/10.1016/j.compositesa.2021.106478.

[31] Gassan J, Chate A, Bledzki AK. Calculation of elastic properties of natural fibers. J Mater Sci 2001;36:3715–20. https://doi.org/10.1023/A:1017969615925.

[32] Nilsson T, Gustafsson PJ. Influence of dislocations and plasticity on the tensile behaviour of flax

and hemp fibres. Compos Part A Appl Sci Manuf 2007;38:1722–8. https://doi.org/10.1016/j.compositesa.2007.01.018.

[33] Roudier A. Analyse multi-échelle du comportement. Université Blaise Pascal - Clermont-Ferrand II, 2012.

[34] Thuault A, Bazin J, Eve S, Bréard J, Gomina M. Numerical study of the influence of structural and mechanical parameters on the tensile mechanical behaviour of flax fibres. J Ind Text 2014;44:22–39. https://doi.org/10.1177/1528083713481835.

[35] Beaugrand J, Guessasma S. Scenarios of crack propagation in bast fibers: Combining experimental and finite element approaches. Compos Struct 2015;133:667–78. https://doi.org/10.1016/j.compstruct.2015.07.119.

[36] Del Masto A, Trivaudey F, Guicheret-Retel V, Placet V, Boubakar L. Nonlinear tensile behaviour of elementary hemp fibres: a numerical investigation of the relationships between 3D geometry and tensile behaviour. J Mater Sci 2017;52:6591–610. https://doi.org/10.1007/s10853-017-0896-x.

[37] Del Masto A, Trivaudey F, Guicheret-Retel V, Placet V, Boubakar L. Investigation of the possible origins of the differences in mechanical properties of hemp and flax fibres: A numerical study based on sensitivity analysis. Compos Part A Appl Sci Manuf 2019;124:105488. https://doi.org/10.1016/j.compositesa.2019.105488.

[38] Guessasma S, Beaugrand J. Damage kinetics at the sub-micrometric scale in bast fibers using finite element simulation and high-resolution X-ray micro-tomography. Front Plant Sci 2019;10:1–11. https://doi.org/10.3389/fpls.2019.00194.

[39] Richely E, Nuez L, Pérez J, Rivard C, Baley C, Bourmaud A, et al. Influence of defects on the tensile behaviour of flax fibres: Cellulose microfibrils evolution by synchrotron X-ray diffraction and finite element modelling. Compos Part C Open Access 2022;9. https://doi.org/10.1016/j.jcomc.2022.100300.

[40] Richely E, Bourmaud A, Placet V, Guessasma S, Beaugrand J. A critical review of the ultrastructure, mechanics and modelling of flax fibres and their defects. Prog Mater Sci 2022;124:100851. https://doi.org/10.1016/j.pmatsci.2021.100851.

[41] Legland D, Beaugrand J. Automated clustering of lignocellulosic fibres based on morphometric features and using clustering of variables. Ind Crops Prod 2013;45:253–61.

https://doi.org/10.1016/j.indcrop.2012.12.021.

[42] Mattrand C, Béakou A, Charlet K. Numerical modeling of the flax fiber morphology variability. Compos Part A Appl Sci Manuf 2014;63:10–20. https://doi.org/10.1016/j.compositesa.2014.03.020.

[43] Otsu, N. A threshold selection method from gray-level histograms. IEEE Trans Syst Man Cybern 1996;9:62–6.

[44] Govilas J, Guicheret-Retel V, Amiot F, Beaugrand J, Placet V, Clévy C. Platen parallelism significance and control in single fiber transverse compression tests. Compos Part A Appl Sci Manuf 2022;159. https://doi.org/10.1016/j.compositesa.2022.106990.

[45] Charlet K, Jernot JP, Breard J, Gomina M. Scattering of morphological and mechanical properties of flax fibres. Ind Crops Prod 2010;32:220–4. https://doi.org/10.1016/j.indcrop.2010.04.015.

[46] Jeannin T, Yung L, Evon P, Labonne L, Ouagne P, Lecourt M, et al. Native stinging nettle (Urtica dioica L.) growing spontaneously under short rotation coppice for phytomanagement of trace element contaminated soils: Fibre yield, processability and quality. Ind Crops Prod 2020;145:111997. https://doi.org/10.1016/j.indcrop.2019.111997.

[47] Govilas J, Clévy C, Beaugrand J, Vincent P. Characterization of plant fiber transverse mechanical behavior using a micromechatronical setup. 5th Int. Conf. Nat. Fibers (ICNF 2021), 2021, p. 2.

[48] Aslan M, Chinga-Carrasco G, Sørensen BF, Madsen B. Strength variability of single flax fibres. J Mater Sci 2011;46:6344–54. https://doi.org/10.1007/s10853-011-5581-x.

[49] Lefeuvre A, Bourmaud A, Morvan C, Baley C. Tensile properties of elementary fibres of flax and glass: Analysis of reproducibility and scattering. Mater Lett 2014;130:289–91. https://doi.org/10.1016/j.matlet.2014.05.115.

[50] Comas-Cardona S, Le Grognec P, Binetruy C, Krawczak P. Unidirectional compression of fibre reinforcements. Part 1: A non-linear elastic-plastic behaviour. Compos Sci Technol 2007;67:507–14. https://doi.org/10.1016/j.compscitech.2006.08.017.

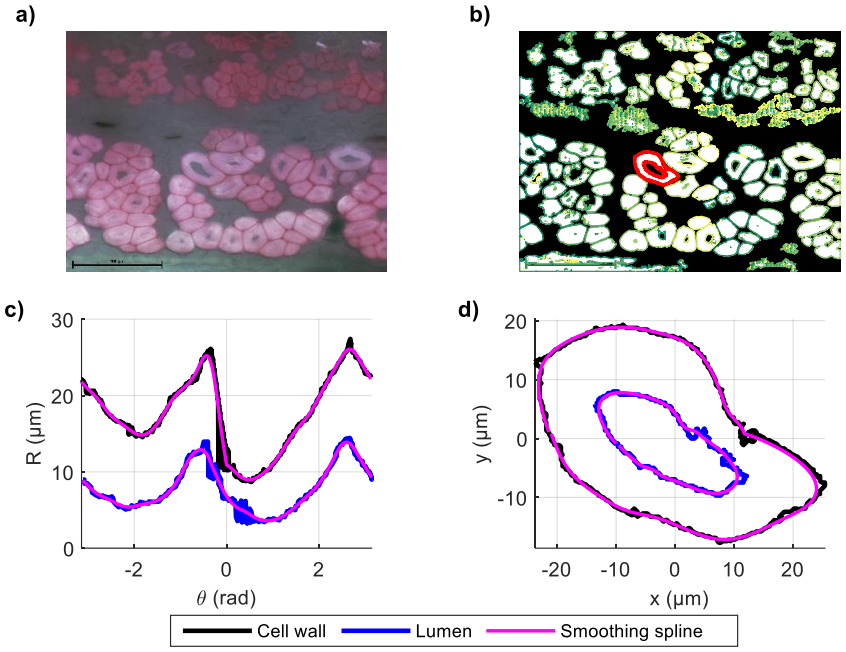

Figure 1: Extraction of plant fiber cross section geometries from microscopy image. a) original microscopy observation of hemp stem section. b) binarization and contour detection (contours are represented in color). c) polar coordinates of cell wall and lumen of the fiber represented in red in b), with applied smoothing spline. d) final smoothed fiber geometry in cartesian coordinates, superimposed over raw data.

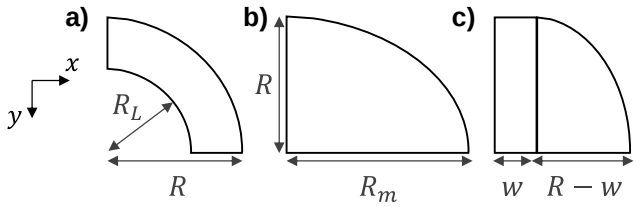

Figure 2: Ideal representations of main plant fiber geometric features: a) circular cross section with circular lumen, b) elliptical cross section, c) flat fiber section. Fibers are considered symmetric along the x and y axis.

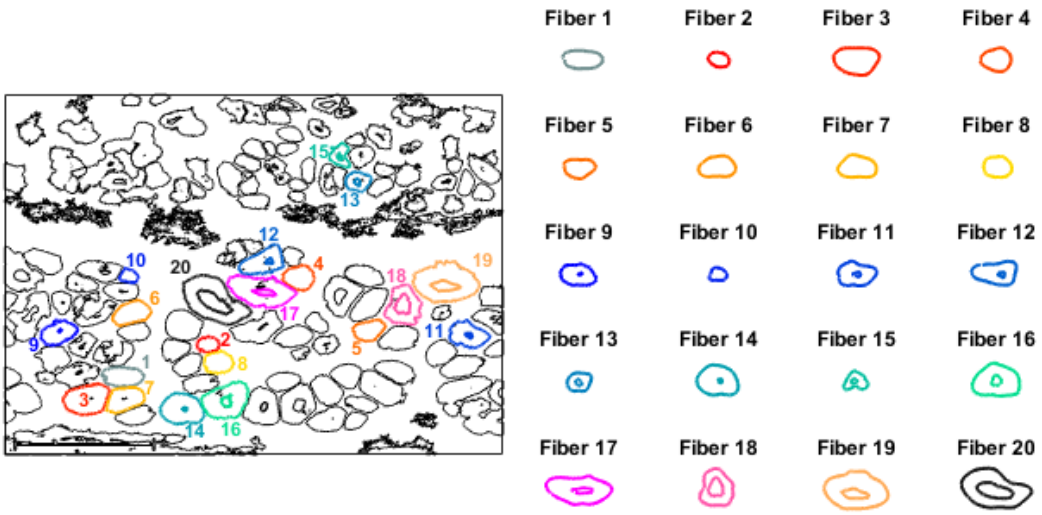

Figure 3: Extracted and smoothed hemp fiber geometries for finite element analysis. Diverse cell wall, lumen shapes and sizes are chosen.

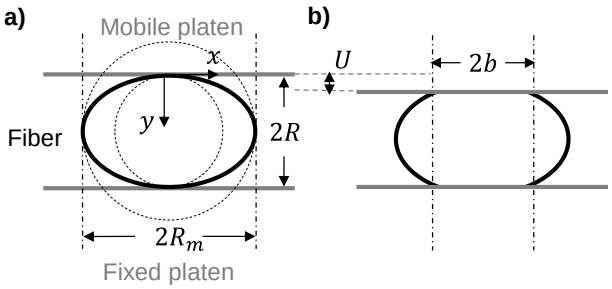

Figure 4: Elliptical cross section fiber under transverse compression, with the fiber's major axis parallel to the compression platens: a) undeformed state, b) deformed state.

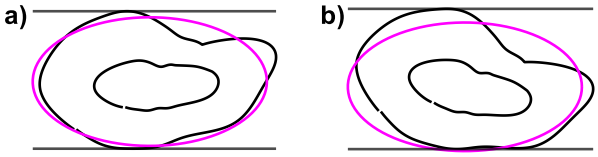

Figure 5: Ellipse fitting and rotation on microscopy-extracted geometries: a) fiber cross section with fitted ellipse after rotation to position the major ellipse axis horizontally, b) user rotation to position fiber in a configuration where partial compression is minimized.

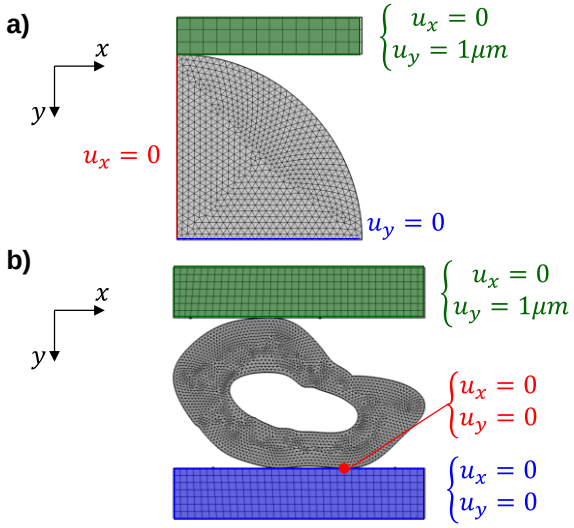

Figure 6: Finite element models of plant fiber SFTCT with mesh and boundary conditions. a) ideal circular geometry, b) microscopy-extracted geometry.

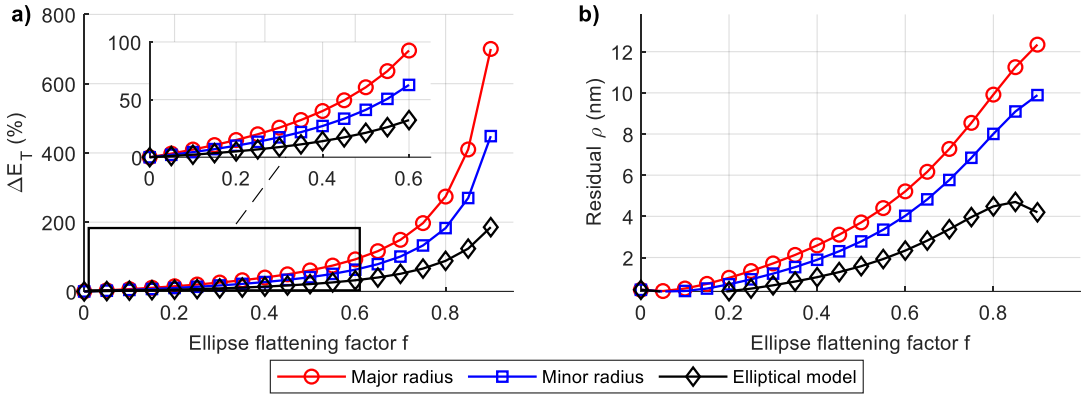

Figure 7:Identification results using elliptical and conventional analytical models as function of ellipse flattening factor f: a) relative difference between identified and imposed transverse elastic modulus ΔE_T, b) average least-squares residual ρ. In the case of the standard model the major or minor radius is given as an input.

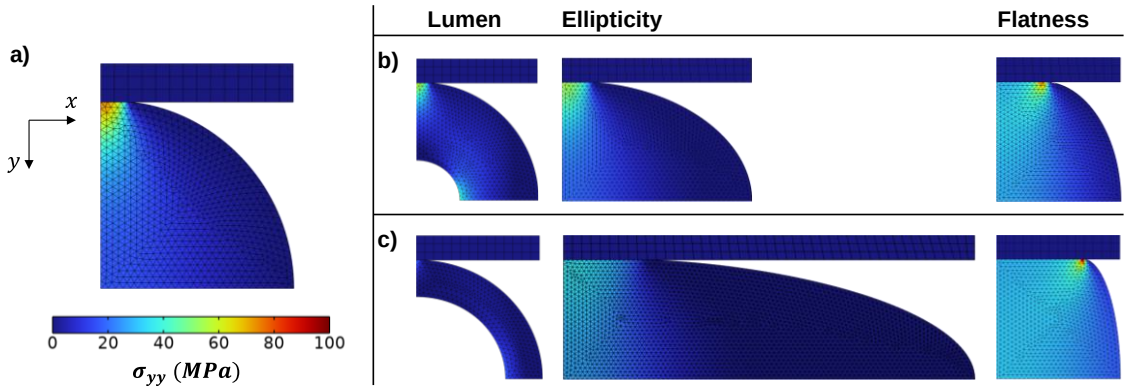

Figure 8: Vertical component of stress field for different ideal fiber geometries: a) circular fiber, b) lumen, elliptical and flat fiber for R_L/R , f , and w/R equal 0.35 c) lumen, elliptical and flat fiber for R_L/R , f , and w/R equal 0.7 .

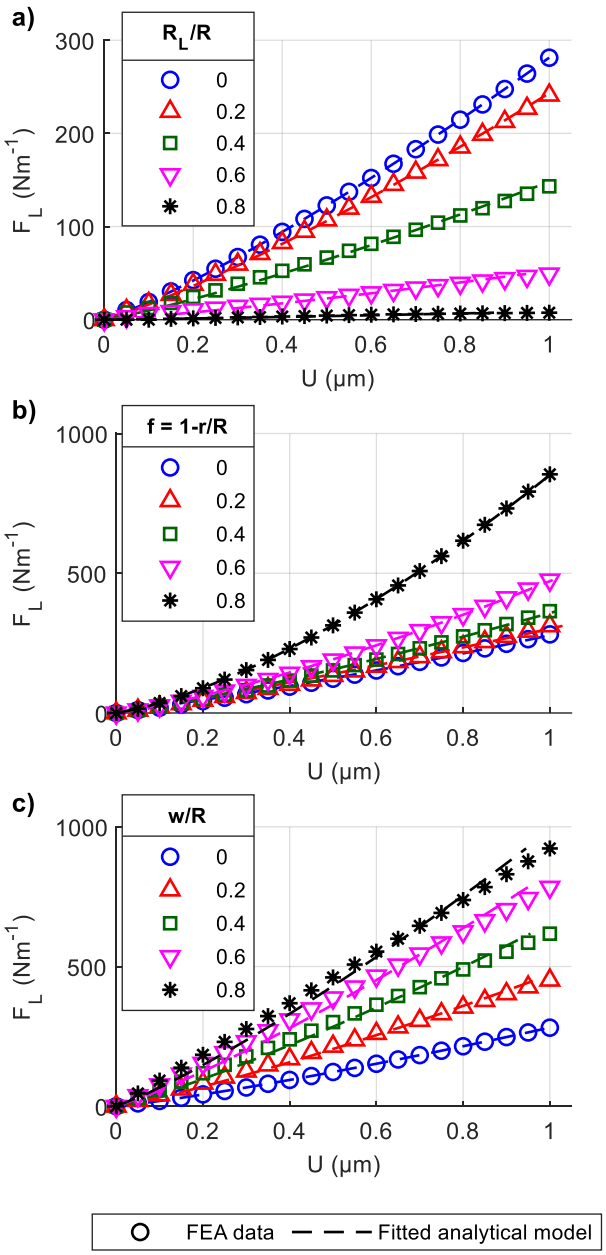

Figure 9: Force per unit length (F_L) and displacement (U) FEA results for ideal plant fiber geometric characteristics: a) lumen, b) ellipticity, c) flat section. FEA analysis is represented with markers while the dotted lines represent the fitted analytical model.

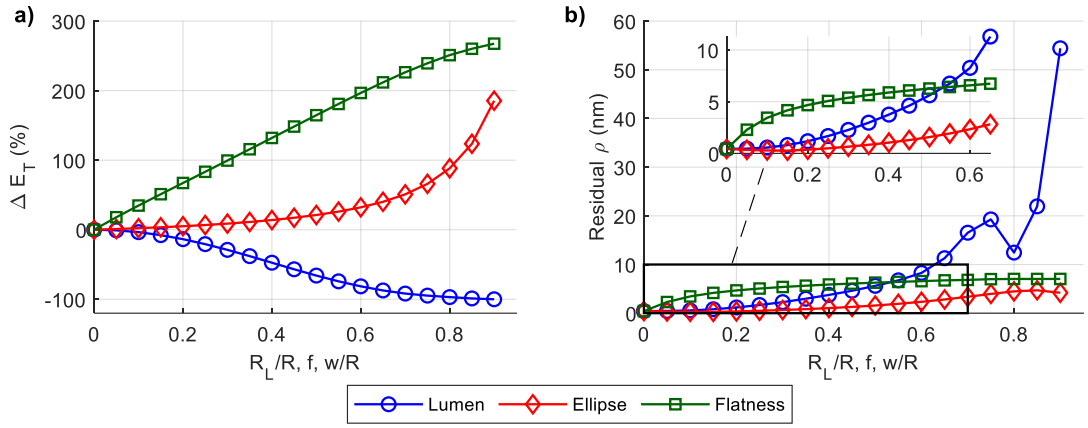

Figure 10: Identification results for plant fiber geometries with ideal geometric characteristics as a function of lumen size (R_L/R), ellipse flattening factor (f) and flat section width (w/R): a) relative difference between identified and imposed transverse elastic modulus ΔE_T, b) average least-squares residual ρ.

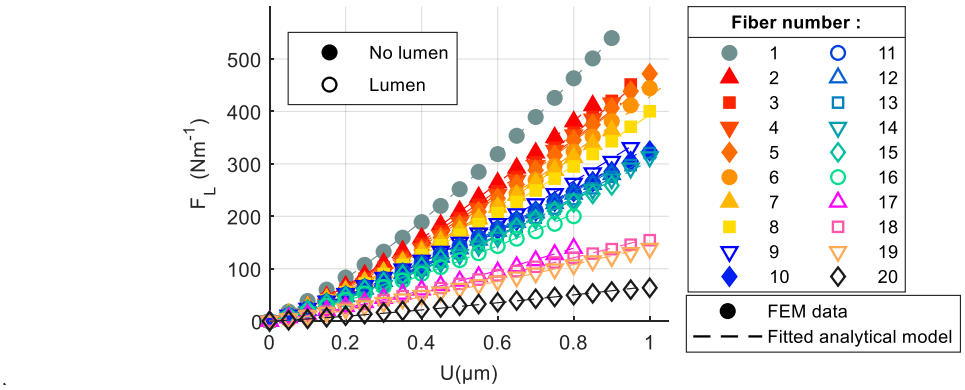

Figure 11: Force per unit length (F_L) and displacement (U) FEA results for microscopy-extracted fibers. FEA analysis data is represented with markers while the dotted lines represent the fitted analytical model. Color filled markers are used for fibers with no lumen and markers with no filling for fibers with a lumen. Occasional removal of initial rotational movement leads to different maximum displacement values between fibers.

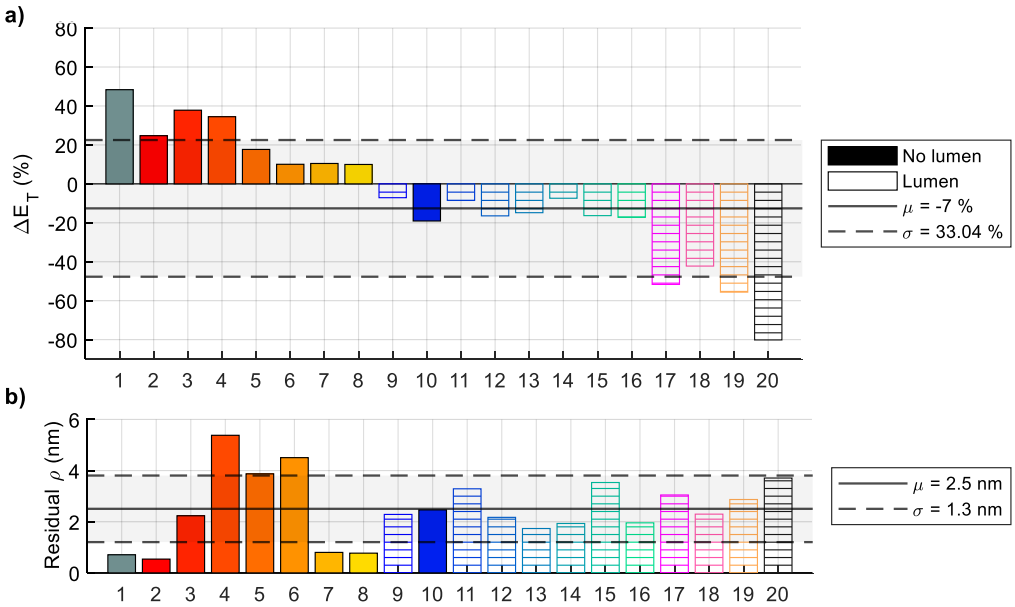

Figure 12:. Identification results for microscopy extracted plant fiber geometries: a) relative difference between identified and imposed transverse elastic modulus ΔE_T, b) average least-squares residual ρ. Color filled bars are used for fibers with no lumen and bars with no filling for fibers with a lumen. Mean (μ) and standard deviation (σ) values are represented with whole and dotted lines respectively.